Available online at www.sciencedirect.com

ScienceDirect

International Journal of Naval Architecture and Ocean Engineering 8 (2016) 22–37
http://www.journals.elsevier.com/international-journal-of-naval-architecture-and-ocean-engineering/

Hydrodynamic analysis of the surface-piercing propeller in unsteady open water condition using boundary element method

Ehsan Yari, Hassan Ghassemi*

Amirkabir University of Technology, Department of Ocean Engineering, Tehran, Iran

Received 25 June 2015; revised 26 August 2015; accepted 15 September 2015
Available online 21 January 2016

Abstract

This article investigates numerical modeling of surface piercing propeller (SPP) in unsteady open water condition using boundary element method. The home code based on BEM has been developed for the prediction of propeller performance, unsteady ventilation pattern and cross flow effect on partially submerged propellers. To achieve accurate results and correct behavior extraction of the ventilation zone, finely mesh has generated around the propeller and especially in the situation intersection of propeller with the free surface. Hydrodynamic coefficients and ventilation pattern on key blade of SPP are calculated in the different advance coefficients. The values obtained from this numerical simulation are plotted and the results are compared with experiments data and ventilation observations. The predicted ventilated open water performances of the SPP as well as ventilation pattern are in good agreement with experimental data. Finally, the results of the BEM code/experiment comparisons are discussed.

Keywords: SPP; BEM; Hydrodynamic coefficients; Ventilation

1. Introduction

A surface piercing propeller is a special type of super-cavitating propeller, which operates at partially submerged conditions. A defect of using SPP is that a complete performance prediction method is still under development and even though SPP are used largely in the boat racing community, the design of SPP is often performed in a trial-and-error basis. The first research activity has been recorded on SPPs was conducted by Shiba (1953). In this research, 2D section of surface propeller with different profiles and the various parameters affecting the ventilation phenomenon were investigated experimentally. During 1970s to 1990s, several experimental tests were conducted on ventilation parameters and their effects on average loss of thrust and efficiency such as Wang (1977), Olofsson (1996), Rose and Kruppa (1991), Kruppa (1992) and Rose et al. (1993). The first application of boundary element method was made for the partially cavitating flow in a two-dimensional foil by Uhlman (1987). A boundary element method based on velocity was used together with a termination wall model, and the cavity surface was iterated until the dynamic and kinematic boundary conditions were satisfied. Shortly after that, BEM based potential was applied for two dimensional cases by Kinnas and Fine (1990) and by Lee et al. (1992).

Pellone and Rowe (1981) calculated the super-cavitating flow on a three-dimensional hydrofoil using a BEM based on velocity and Pellone and Pellat (1995) extended the same method for partial cavities. Propeller wetted flow calculation using BEM based on velocity is performed due to Hess and Valarezo (1985) and with a potential based BEM by Lee (1987). The work done at MIT in the 90s on BEMs considerably advanced the application of the BEM to propeller flows: the work of Hsin (1990) for the unsteady wetted propeller flow and the work of Fine (1992) for the unsteady cavitating flow

* Corresponding author.
E-mail address: gasemi@aut.ac.ir (H. Ghassemi).
Peer review under responsibility of Society of Naval Architects of Korea.

http://dx.doi.org/10.1016/j.ijnaoe.2015.09.002

on propellers. Similar work has been carried out by Kim et al. (1994) and Kim and Lee (1996). The innovative work of Fine was then followed by Kinnas and Fine (1992) and a series of extensions and enhancements on the application of the BEMs to cavitating-ventilating flow on propellers was done by Kinnas and his group: surface piercing propellers by Young and Kinnas (2002), mid-chord cavitation by Mueller (1998), ducted propellers by Kinnas et al. (2003), rudder and propeller cavitation interaction by Lee et al. (2003), hydro-elastic analysis of cavitating propellers by Young (2003), and tip vortex cavitation modeling by Lee and Kinnas (2002).

The first modeling of surface piercing propeller was carried out by Oberembt (1968). He used a lifting line method to calculate the characteristics of SPPs. Oberembt (1968) assumed that the propeller is lightly loaded such that no natural ventilation of the propeller and its vortex wake occur. A lifting-line approach which includes the effect of propeller ventilation was developed by Furuya (1985). He used linearized boundary conditions to account for free surface effects. The blades were reduced to a series of lifting lines, and method was combined with a 2-D water entry-and-exit theory developed by Wang (1979), Wang et al. (1990, 1992) to determine thrust and torque coefficients. Furuya compared the predicted mean thrust and torque coefficients with experimental measurements obtained by Hadler and Hecker (1968). In general, the predicted thrust coefficients were within acceptable range compared to measured values. However, there were significant discrepancies with torque coefficients. Furuya attributed the discrepancies to the effects of nonlinearity, absence of the blade and cavity thickness representation in the induced velocity calculation, and uncertainties in interpreting the experimental data.

One of the numerical studies related to this topic was the prediction of the flow around surface piercing hydrofoil by time marching boundary element method that was carried out by Savineau and Kinnas (1995), Savineau (1996). In this research the non-linear cavity geometry is determined iteratively by applying the kinematic boundary condition on the exact cavity surface at each time step. According to the obtained results, the developed two-dimensional method is very efficient at predicting the cavity geometry and pressure distributions during the entry phase and thus can be used as a basis to design SPP blades.

Young and Kinnas (2003) extended a 3D boundary element method which was developed in the past for the prediction of unsteady sheet cavitation on conventional fully submerged propellers to predict the performance of super-cavitating and SPP. Then, Koushan (2004) presented his research about total dynamic loadings of ventilated propellers, and showed that fluctuations during one ventilation cycle can range from 0 to 100% of the average force of a non-ventilated propeller. Ghassemi (2009) used a practical numerical method to predict the hydrodynamic characteristics of the SPP. The critical advance velocity ratio is derived using the Weber number and pitch ratio in the transition mode, then the potential based boundary element method (BEM) was used on the engaged surfaces.

Following Koushan' research, numerical simulation was performed for different types of propeller ventilation by Califano and Steen (2009). This research aimed at analyzing the ventilation mechanism. The commercial RANS code was used to solve the viscous, incompressible, two-phase flow. In terms of both thrust forces and air content, the present analysis shows a satisfactory agreement with the filtered experimental data during the first half revolution. Classification of different types of propeller ventilation and ventilation inception mechanism based on analysis of a series of experiments were investigated by Kozlowska et al. (2009). Three different types of ventilation inception mechanisms were observed based on experimental results. Vinayan and Kinnas (2008, 2009) solved the flow field around a ventilated two-dimensional surface piercing hydrofoil and propellers using a robust nonlinear boundary element method. Results are presented for the fully wetted and ventilated cases with and without the effects of gravity, simulating the effect of changes in the Froude number. A series of four-bladed propellers of the surface piercing type was developed to design a SPP for a given operating condition by Misra et al. (2012). According to the Misra results, the best performance at all immersions was obtained from the propeller using wedge shaped sections with the trailing edge inclined at 60° to the horizontal axis. Only a propeller series with four blades has been developed in this work. Numerical analysis of surface piercing propeller using RANS method was extracted by Himei (2013). In this study analysis program using potential flow theory for supercavitating propeller was diverted for surface piercing propeller. Based on numerical results, RANS simulations have good agreement with experimental results.

The main target of this study is development of home code based on boundary element method for the prediction of propeller performance, unsteady ventilation pattern and cross flow effect on partially submerged propellers. In order to validation the numerical data, analysis of 841-B surface piercing propeller that experimental measurements are available has been done in unsteady open water condition under the free surface condition. All calculations were done at zero shaft yaw and inclination angle. The amounts of force/moment components of key blade in a revolution of the SPP calculated and have been compared with experimental data. Finally the results of pressure coefficients and ventilation pattern on the propeller and key blade have been discussed.

1.1. SPP-841B propeller

In this paper, numerical simulation of SPP-841B propeller model has been investigated that the test data of it, is available. All calculations have been done at $I = 0.33$ and zero shaft yaw and inclination angle. The immersion ratio ($I = h/D$) affects the values of K_T and K_Q since the thrust and torque depend on how much of the propeller blade is in water during each revolution, and this depends upon the immersion of the propeller. The immersion ratio is defined as the ratio of the blade tip immersion to the propeller diameter. Where h is the blade tip immersion and D is the propeller diameter. The actual geometry and modeling is similar to Fig. 1. Geometrical characteristics of the propeller are shown in Table 1.

2. EXPERIMENTAL work DESCRIPTION

Model experiments in the free-surface cavitation tunnel are conducted on a partially submerged propeller designed for high speed operation. With the objective to carry out unsteady force measurements on an individual blade of a partially submerged propeller, in combination with observation of the accompanying flow, for a large set of test conditions an extensive model test program was established. This section presents the choice of an appropriate facility for this type of test, the propeller selected prototype, special instrumentation, and test conditions. Procedures for the force measurements and the flow observation are also described. The free-surface cavitation tunnel was selected for several reasons. First, model testing of partially submerged propellers obviously necessitates a free water surface. Hence a free-surface facility was required, which in turn left the choice either to a towing tank or a cavitation tunnel of the free surface type. Secondly, bearing in mind that one objective of the tests was to study in detail the flow accompanying an operating partially submerged propeller, a cavitation tunnel makes flow observation easy and possible for any period of time.

The large test section with a width of 0.8 m and the water-filled height of 0.8 m ensures small wall effects under fully cavitating or ventilated conditions, which otherwise would cause flow blockage and amplified surface elevation in a smaller tunnel. Also, the test section length of 4 m and the distance of 0.7 m from the free surface to the covering hatch permits spray to develop more or less unrestrained as it trails downstream. A unique test apparatus was designed, permitting the shaft to be yawed over a range of angles, independently inclined, and dynamic blade forces to be measured by means of a blade dynamometer. The shaft orientation unit is a device that permits the propeller shaft to be yawed and set by remote control at any yaw angle between ±30°, while the shaft may have an inclination from the horizontal.

The propeller, that has adjustable-pitch blades and a hub containing a blade dynamometer, is driven from aft by the right-angle gear drive unit via two constant-velocity joints connected by a short hollow intermediate shaft. The actual yaw angle is picked up by a sensor situated at the lower end of the pivot, and the absolute angular position of the propeller is provided by a pulse transducer connected to the upstream end of propeller shaft. A flat plate spanning the tunnel width in front of the propeller provides a well defined free surface. The blade dynamometer was an existing 4-bladed, single flexure, 5-component dynamometer. This dynamometer had been specifically designed for dynamic measurements of loads and given exceptional characteristics.

Table 1
Particulars of propeller model of the SPP-841B.

Parameter	Symbol	Value
Diameter (mm)	D	250
Hub diameter (mm)	d	85
Pitch at 0.7 radius (mm)	P	310
Hub-diameter ratio	d/D	0.34
Pitch-diameter ratio at 0.7 radius	P/D	1.24
Expanded Area ratio	A_E/A_0	0.58
Number of blades	Z	4
Rotation	R.H.	

3. Mathematical modeling of the problem

The formulation of the equations and the boundary conditions for the three-dimensional unsteady partially and fully ventilating flow using boundary element method based on potential flow problem is presented. The particular cases of three-dimensional flow, unsteady flow conditions are derived from the general formulation. Additional considerations are made on the modeling of the relevant physical phenomena such as ventilation and free surface. In continue, the complete problem definition is presented. A boundary integral method based potential flow involving Green's function is used to solve the boundary value problem. The complete boundary condition on the body, ventilation surface, free surface and wake sheet are derived in detail and the needed simplification is justified. Let the external flow domain Ω extend to infinity and be bounded by the boundary S and the unit vector of $\vec{n}$ normal to S as shown in Fig. 2. Boundary S of the flow region includes the surface of the body S_B, the surface of the wake S_W, and the outer surface S_∞ that surround the surfaces of the body and the trailing vortex surface.

Two reference frames are considered as Fig. 2 that a Cartesian inertial reference frame (X, Y, Z) fixed in space; and a body-attached reference frame described by Cartesian coordinates (x, y, z). Assuming the flow in the domain external to

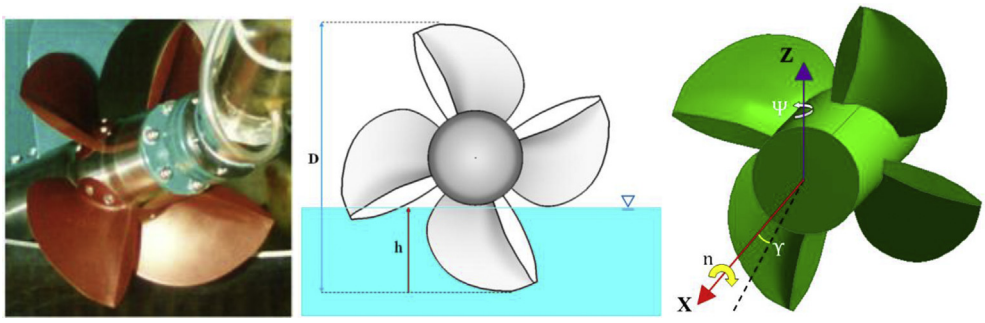

Fig. 1. SPP-841B propeller and BEM model in addition definitions of yaw angle Ψ, immersion ratio I = h/D, shaft inclination shaft angle γ and SPP rate of revolution.

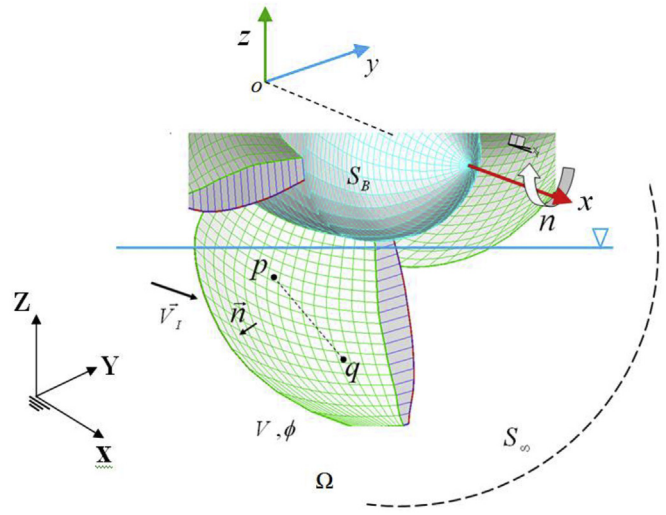

Fig. 2. The propeller typical geometries and the coordinate reference systems (inertial system and body-attached system).

the SPP and ventilated surfaces to be effectively inviscid, incompressible and irrotational. The disturbance velocity is irrotational with the exception of the surfaces of discontinuity of the velocity field which constitute the wakes of lifting surfaces replace it. Therefore the disturbance velocity, being irrotational, may be written as the gradient of the disturbance potential $\phi(x,t)$, $\boldsymbol{V}(x,t) = \nabla\phi(x,t)$. For an incompressible flow field, the continuity equation equal $\nabla\cdot\boldsymbol{V}(x,t) = 0$.

$$\nabla^2\phi\,(x,t) = 0 \tag{1}$$

The total velocity at any point of the flow domain, $\boldsymbol{V}$, is the sum of the undisturbed velocity and the disturbance velocity:

$$\boldsymbol{V}(\mathrm{x},\mathrm{t}) = \boldsymbol{V}_0(\mathrm{x},\mathrm{t}) + \nabla\phi\,(x,t) \tag{2}$$

For an incompressible, inviscid and irrotational flow the Navier–Stokes momentum equations reduce to the Bernoulli equation. In the body-attached reference system, the unsteady Bernoulli equation reads:

$$\frac{\partial\phi}{\partial t} + \frac{p}{\rho} + \frac{|\boldsymbol{V}|^2}{2} + gz = \frac{p_{ref}}{\rho} + \frac{|\boldsymbol{V}_0|^2}{2} \tag{3}$$

In Eq. (3), p, ρ and p_{ref} are pressure, fluid density and reference pressure of the fluid, respectively. For a propeller, p_{ref} is the pressure far upstream and it obeys to the hydrostatic law, $p_{ref} = p_{atm} + \rho gz$ being p_{atm} the atmospheric pressure at the depth of free surface. Reference (V_{ref}) speed are usually considered as the resultant vector of inlet velocity and rotational speed (nD). D is the propeller diameter and n is the rotational speed (revolution per second). V_{ref} is defined as:

$$V_{ref} = \sqrt{V_0^2 + (\omega xR)^2} \quad where \quad (x = r/R\,,\omega = 2\pi n) \tag{4}$$

The unsteady Bernoulli Eq. (3) can be rewritten as:

$$\frac{2}{V_{ref}^2}\frac{\partial\phi}{\partial t} + \frac{|\boldsymbol{V}|^2 - |\boldsymbol{V}_0|^2}{V_{ref}^2} + \frac{2gz}{V_{ref}^2} = -C_p \tag{5}$$

4. Boundary conditions

A 3-D potential based BEM is used for the numerical modeling of surface-piercing propellers. At each time step, a Fredholm integral equation of the second kind is solved with respect to the perturbation potential. A Dirichlet type boundary condition is applied on the ventilating surfaces, and a Neumann type boundary condition is applied on the wetted surfaces. The general formulation for the prediction of SPP ventilation pattern in unsteady open water condition is presented in this section. The boundary surface S divided into Body surface (S_B), ventilated surface (S_V), Wake surface (S_W) and Surface at infinity (S_∞). S_B is the wetted part of the propeller without ventilation; S_V is the Portion of propeller surface subjected to ventilation; S_W is a sheet following the lifting bodies at downstream and S_∞ represents a surface at infinity. For the wetted part of the body surface S_B the condition of zero normal velocity components is satisfied by imposing the Neuman boundary condition:

$$\frac{\partial\phi}{\partial n} = -\boldsymbol{V}_0\cdot\boldsymbol{n} \tag{6}$$

Where n is the unit normal vector defined outward from the boundary surface S.

• Kinematic Boundary Condition on Ventilated Surfaces

The kinematic boundary condition on the ventilated surfaces requires the total velocity normal to the ventilated surfaces to be zero, which renders the following equation for the ventilation thickness (η) on the blade:

$$\frac{\partial\eta}{\partial S_1}(V_{s1} - V_{s2}cos\theta) + \frac{\partial\eta}{\partial S_2}(V_{s2} - V_{s1}cos\theta) = (sin\theta)^2\left(V_{s3} - \frac{\partial\eta}{\partial t}\right), \quad \text{on } S_V \tag{7}$$

η is the ventilation thickness function in non-orthogonal local coordinate system and t is time parameter. s_1, s_2 and s_3 are curvilinear directions element-fitted in non-orthogonal reference system with unit base vectors $(\boldsymbol{t}_1, \boldsymbol{t}_2, \boldsymbol{t}_3)$ as follow (see Fig. 3).

• Dynamic Boundary Condition

The DBC states that the pressure on the ventilated surface equals the atmospheric pressure, $p = p_{atm}$. The dynamic boundary condition Eq. (5) is formulated taking into account Eq. (8):

$$\left|\boldsymbol{V}\right|^2 = V_{ref}^2\,\sigma + \left|\boldsymbol{V}_0\right|^2 - 2gz - 2\frac{\partial\phi}{\partial t} \quad on\ S_V \tag{8}$$

In the non-orthogonal reference system, this equation is:

$$\left[\frac{1}{|\boldsymbol{t}_1\times\boldsymbol{t}_2|(V_{s_1} - (\boldsymbol{t}_1\cdot\boldsymbol{t}_2)V_{s_2})}\right]^2 + V_{S_2}^2 + V_{S_3}^2 = V_{ref}^2\sigma + \left|\boldsymbol{V}_0\right|^2 - 2gz \tag{9}$$

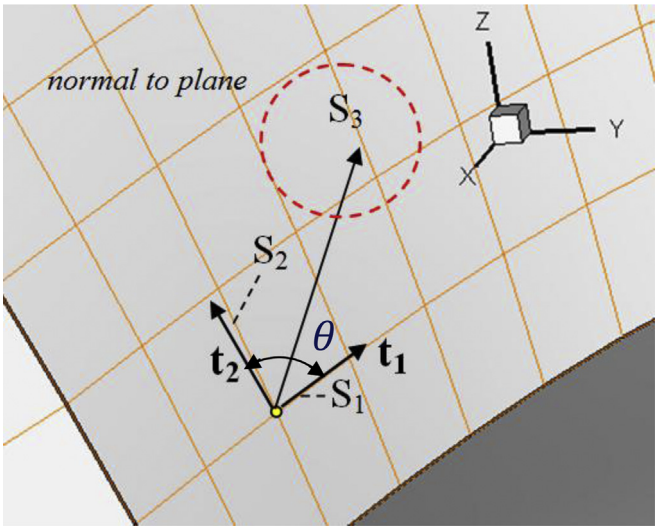

Fig. 3. Local non-orthogonal coordinate reference system (s_1, s_2, s_3) and θ is the angle between the non-orthogonal tangent unit vectors $\mathbf{t}_1$ and $\mathbf{t}_2$.

The dynamic boundary condition is non-linear on ϕ due to the presence of quadratic terms on the perturbation potential spatial derivatives. Dynamic boundary condition may be changed to Dirichlet boundary condition on ϕ. So, for V_{s_1}, the following equation is obtained.

$$V_{s_1} = V_{s_2}cos\theta + sin\theta\sqrt{V_{ref}^2\sigma + \left|\boldsymbol{V}_0\right|^2 - 2gz - 2\frac{\partial\phi}{\partial t} - V_{S_2}^2 - V_{S_3}^2} \tag{10}$$

By integrating along S_1 from flow detachment point, $s_{l_0} = s_0$, and considering the potential value ϕ, following equation is extracted for ϕ.

$$\phi = \phi_0 + \int_{s_{l0}}^{s_l}\left[V_{s_2}cos\theta + sin\theta\sqrt{V_{ref}^2\,\sigma + |\boldsymbol{V}_0|^2 - 2gz - 2\frac{\partial\phi}{\partial t} - V_{S_2}^2 - V_{S_3}^2} - \boldsymbol{V}_0\cdot\boldsymbol{t}_1\right]ds_1 \;\; on\; S_V \tag{11}$$

- Wake surface and Surface at infinity

The wake surface consists of the surface carrying all the vorticity shed by the lifting surface to which it is attached. It is a zero thickness vortex layer, or vortex sheet. Wake surface must satisfy dynamic and kinematic boundary condition. To satisfy the kinematic boundary condition, vortex wake s_W should be as a surface of zero thickness. If $\boldsymbol{V}_n$ indicates the velocity of wake surface in the normal direction, then kinematic boundary condition for unsteady flow is:

$$\boldsymbol{V}^+\cdot\boldsymbol{n} = \boldsymbol{V}^-\cdot\boldsymbol{n} = \boldsymbol{V}_m\cdot\boldsymbol{n} = \boldsymbol{V}_n \tag{12}$$

$\boldsymbol{V}_m$ is the average velocity of the fluid. According to dynamic boundary condition, pressure difference in two sides of wake surface is zero. The surface S_∞ is a control surface and is chosen as the surface of a hemisphere of large radius. So the integral over the surface S_∞ must be zero as the radius of hemisphere increases infinitely

- Kutta Condition

The wake surface S_w is assumed to have zero thickness. The normal velocity jump and the pressure jump across S_w is zero, while a jump in the potential is allowed (Huang et al., 2007).

$$(\Delta p)_{on\ S_w} = p^+ - p^- = 0 \tag{13}$$

$$\Delta\left(\frac{\partial\phi}{\partial n}\right)_{on\ S_w} = \left(\frac{\partial\phi}{\partial n}\right)^+ - \left(\frac{\partial\phi}{\partial n}\right)^- = 0$$

A Kutta condition is required at the trailing-edge to uniquely specify the circulation. In its most general form, it states that the flow velocity at the trailing-edge remains bounded

$$\left|\nabla\phi\right|_{TE} < \infty$$

- Free-surface condition

The method of negative imaging is used to enforce the free surface boundary condition. The imaged cross-section of blade and ventilated surface, shown in Fig. 4, is represented by sinks and dipoles with opposite normal. The kinematic and dynamic boundary conditions on the free surface can be written as:

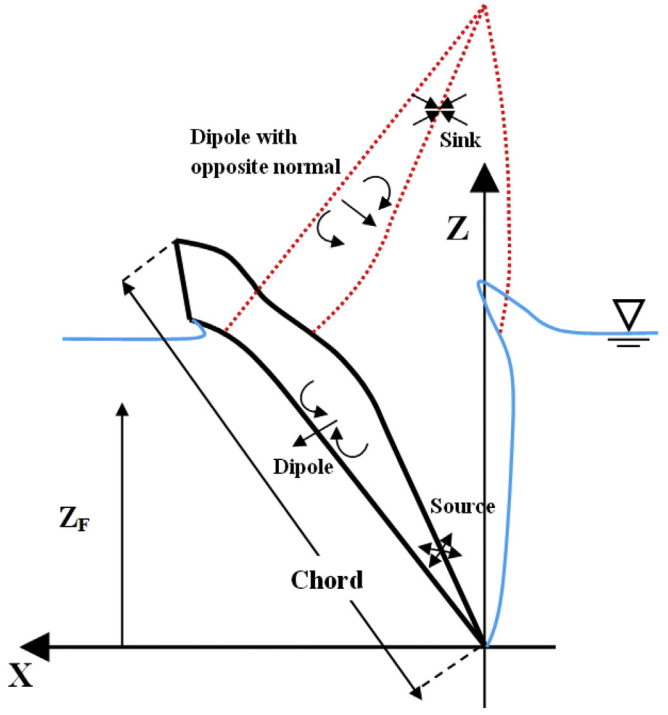

Fig. 4. Perturbation potential distribution on blade section, ventilation surface and their images.

$$\phi_x\varsigma_x+\phi_y\varsigma_y-\phi_z=0 \quad at\ z=\varsigma$$
$$g\varsigma+\frac{1}{2(\nabla\phi\cdot\nabla\phi-V^2)}=0 \quad at\ z=\varsigma \tag{14}$$

$$\nabla\phi\cdot\nabla\left[\frac{1}{2(\nabla\phi\cdot\nabla\phi)}\right]+g\phi_z=0 \quad at\ z=\varsigma \tag{15}$$

The free-surface boundary condition is nonlinear in nature and should be satisfied on the true surface, which is unknown and can be linearized as a part of the solution using the perturbation method. Substituting Eq. (14) in Eq. (15) and expanding the potential ϕ in a Taylor series about the mean free surface, the first-order free-surface boundary conditions can be obtained as follows:

$$\frac{\partial^2\phi}{\partial t^2}(x,y,z,t)+g\frac{\partial\phi}{\partial y}(x,y,z,t)=0 \quad at \quad z=0 \tag{16}$$

The assumption that the Froude number grows without bounds is valid because surface piercing propellers usually operate at very high speeds. Studies by Shiba have also shown that the effect of Froude number ($F_n=\frac{n\,D}{\sqrt{gD}}$) is negligible for $Fn>2$ in the fully ventilated regime. Assuming that the infinite Froude number condition $Fn\to\infty$ applies, Eq. (16) reduces to:

$$\phi(x,y,z,t)=0 \quad at \quad z=z_F \tag{17}$$

5. Integral equations

Velocity potential in fluid domain Ω is obtained using classic integral. Based on Green's third identify equation ϕ can be written as

$$2\pi\phi_p(t)=\int_{s_B+s_V}\left[\phi_q(t)\frac{\partial G(p:q)}{\partial \boldsymbol{n}_q}-G(p:q)\frac{\partial\phi_q(t)}{\partial \boldsymbol{n}_q}\right]ds+\int_{s_W}\left[\Delta\phi(t)\frac{\partial G(p:q)}{\partial \boldsymbol{n}_q}\right]ds \tag{18}$$

Where p is a field point, q is a singularity point, n_q is normal vector in p. $G(p:q)$ is a proper Green's function for a 3-dimensional analysis of fluid flow that defined as:

$$G(p:q)=\frac{1}{r(p:q)}+\frac{1}{r'(p:q)} \quad , \quad wherer \quad (p:q)=|\boldsymbol{r}| \tag{19}$$

where $r=\sqrt{(x-\zeta)^2+(y-\eta)^2+(z-\xi)^2}$ is the distance between the field point $p(x,y,z)$ and the point of singularity $q(\zeta,\eta,\xi)$, and $r'=\sqrt{(x-\zeta)^2+(y-\eta)^2+(z+\xi)^2}$ (Fig. 2).

In the state of partially submerged propeller, the total number of elements is equal to those of the body that include blades, ventilated surfaces. The discrete form of integral Eq. (18), in the unsteady condition and uniform inflow is:

$$\begin{aligned}&\sum_{K=1}^{Z}\left[\sum_{j=1}^{N_j}\left[\sum_{i=1}^{i_w-1}D_{nij}(t)\,\phi_{ij}(t)+\sum_{i=i_w}^{N_i}D_{nij}(t)\phi_{ij}(t)-\sum_{i=1}^{i_w-1}D'_{nij}(t)\,\phi_{ij}(t)-\sum_{i=i_w}^{N_i}D'_{nij}(t)\phi_{ij}(t)\right]+\sum_{i=1}^{N_{wj}}\left(W_{nj}(t)\Delta\phi_j(t)\right)-\sum_{i=1}^{N_{wj}}\left(W'_{nj}(t)\Delta\phi_j(t)\right)\right]\\&=\sum_{K=1}^{Z}\sum_{j=1}^{N_j}\left[\sum_{i=1}^{i_w-1}S_{nij}(t)\left(\frac{\partial\phi}{\partial n}\right)_{ij}(t)+\sum_{i=i_w}^{N_i}S_{nij}(t)\left(\frac{\partial\phi}{\partial n}\right)_{ij}(t)-\sum_{i=1}^{i_w-1}S'_{nij}(t)\left(\frac{\partial\phi}{\partial n}\right)_{ij}(t)-\sum_{i=i_w}^{N_i}S'_{nij}(t)\left(\frac{\partial\phi}{\partial n}\right)_{ij}(t)\right],\ n\\&=1,.,N_{total}\end{aligned} \tag{20}$$

The indices i, j and n map quantities to panel elements. n is control point and i,j denote location of field point. K is the index of analyzed surfaces (back-face blades and wake surface), N_i is the number of divisions in the direction of blade chord, N_j is the number of divisions in the radial direction of the blade, N_{wj} is the number of wake panels, i_w is the index of element in the direction of chord in which wetted (without ventilation), N_i-i_w+1 is the number of elements under the ventilation in chord direction. The influence coefficients matrices are D_{nij}, D'_{nij}, S_{nij}, S'_{nij}, W_{nij}, W'_{nj} respectively for the body dipoles, body sources, wake dipoles and its image. They are defined as:

$$D=\begin{cases}\frac{1}{2\pi}\int_S\frac{\boldsymbol{r}\cdot\boldsymbol{n}}{|\boldsymbol{r}|^3}dS & n=m\\ 1+\frac{1}{2\pi}\int_S\frac{\boldsymbol{r}\cdot\boldsymbol{n}}{|\boldsymbol{r}|^3}dS & n\neq m\end{cases},S=-\frac{1}{2\pi}\int_S\frac{1}{|\boldsymbol{r}|}dS\,,W=\frac{1}{2\pi}\int_S\frac{\boldsymbol{r}\cdot\boldsymbol{n}}{|\boldsymbol{r}|^3}dS_W \tag{21}$$

Re-arranging Eq. (20) for the unknown quantities, dipole strength on the wetted surface and source strength on the ventilated surface in the left hand side and the known quantities, source strength on the wetted surface and dipole strength

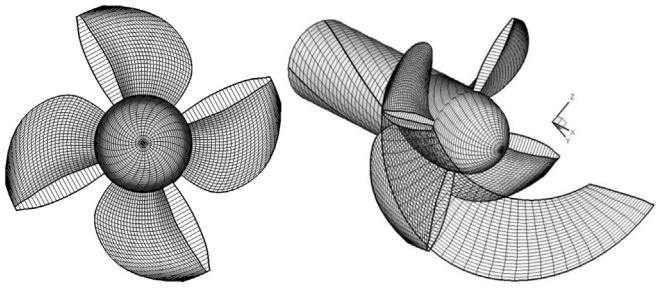

Fig. 5. 841-B surface piercing propeller geometry, fine grid and prescribed wake.

on the ventilated surface in the right hand side, we obtain the following system of equations:

$$\begin{aligned}&\sum_{K=1}^{Z}\left[\sum_{j=1}^{N_j}\left[\sum_{i=1}^{i_w-1}D_{nij}(t)\,\phi_{ij}(t)-\sum_{i=1}^{i_w-1}D'_{nij}(t)\,\phi_{ij}(t)\right.\right.\\&\left.+\sum_{i=i_w}^{N_i}S_{nij}(t)\left(\frac{\partial\phi}{\partial n}\right)_{ij}(t)-\sum_{i=i_w}^{N_i}S'_{nij}(t)\left(\frac{\partial\phi}{\partial n}\right)_{ij}(t)\right]\\&\left.+\sum_{i=1}^{N_{wj}}\left(W_{nj}(t)\Delta\phi_j(t)\right)-\sum_{i=1}^{N_{wj}}\left(W'_{nj}(t)\Delta\phi_j(t)\right)\right]\\&=\sum_{K=1}^{Z}\sum_{j=1}^{N_j}\left[\sum_{i=1}^{i_w-1}S_{nij}(t)\left(\frac{\partial\phi}{\partial n}\right)_{ij}(t)-\sum_{i=1}^{i_w-1}S'_{nij}(t)\left(\frac{\partial\phi}{\partial n}\right)_{ij}(t)\right.\\&\left.+\sum_{i=i_w}^{N_i}D_{nij}(t)\phi_{ij}(t)-\sum_{i=i_w}^{N_i}D'_{nij}(t)\phi_{ij}(t)\right],\ n\\&=1,.,N_{total}\end{aligned}\tag{22}$$

In short, the above equation can be expressed as follows:

$$[A][X]=[B][Y]$$

where [A] and [B] are the influence coefficient matrices, [X] in the vector of unknown and [Y] is the vector of known values. The matrices [A] and [B] are square and full. At any time step NTIME, the [A] and [B] matrices are of size (2 NTIME)*(2 NTIME), and the vectors [X] and [Y] are of size (2 NTIME). The linear system of equations can be written as:

$$[\mathrm{LHS}]\begin{bmatrix}\phi_{wet}\\\left(\frac{\partial\phi}{\partial n}\right)_{ventilation}\\\Delta\phi_{wake}\end{bmatrix}=[\mathrm{RHS}]\tag{23}$$

6. Propeller performance coefficients

After solving the system of equations and extraction the potential value of each surface element, pressure distributions can be calculated directly via Bernoulli's equation:

$$\begin{cases}\left(\overrightarrow{V}_t\right)_i=(\nabla\phi)_i\\p_i=\rho\left(\frac{\partial\phi}{\partial t}\right)_i+0.5\rho\left(2\left(\overrightarrow{V}_I\right)_i.\left(\overrightarrow{V}_t\right)_i-\left(\overrightarrow{V}_t\right)_i.\left(\overrightarrow{V}_t\right)_i\right)\end{cases}\tag{24}$$

Table 2
Flow conditions in various advance coefficients.

J	V(m/s)	I (immersion ratio)
0.4	3.13	0.33
0.5	3.13	0.33
0.7	3.13	0.33
0.8	3.13	0.33
1.2	3.13	0.33
1.3	3.13	0.33

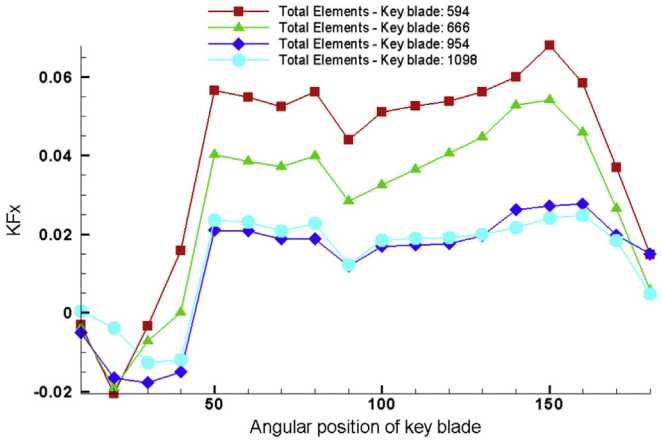

Fig. 6. Convergence of 841-B propeller thrust coefficient versus angular position of key blade in various number of key blade total elements at J = 0.5.

where ρ is the density of the fluid and $\overrightarrow{V}_t$ is tangency velocity component of i th element.

Thrust and torque of the propeller with two components of pressure and friction are expressed as follows:

$$\begin{aligned}Thrust(T)&=\sum_{K=1}^{Z}\sum_{i=1}^{N_{total}}p_i n_{xi}\Delta s_i-F_D\\Torque(Q)&=\sum_{K=1}^{Z}\sum_{i=1}^{N_{total}}p_i\left(n_{yi}\,z_i-n_{zi}\,y_i\right)\cdot s_i+Q_D\end{aligned}\tag{25}$$

The frictional coefficient C_f for the frictional component of thrust F_D and torque Q_D of the propeller can be expressed by the Prantle-Schlichting

$$C_f(j)=\left(1+\frac{t_{max}(j)}{C(j)}\right)\frac{0.455}{\left(Log_{10}^{Re_j}\right)^{2.58}}\tag{26}$$

where $C_f(j)$, $t_{max}(j)$, $C(j)$ and Re_j are the local skin friction coefficient that is calculated from two-dimensional boundary layer theory, maximum thickness of 2D cylindrical cross-section of blade, chord value at any cross-radial and Reynolds number respectively. Reynolds number is calculated as follow:

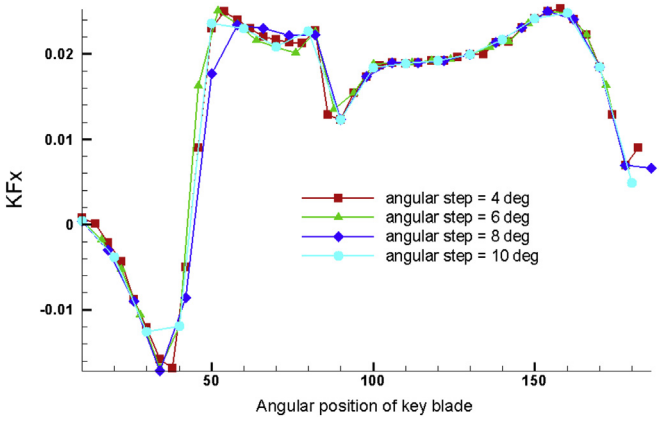

Fig. 7. Convergence of 841-B propeller thrust coefficient versus angular position of key blade in various time step size at J = 0.5.

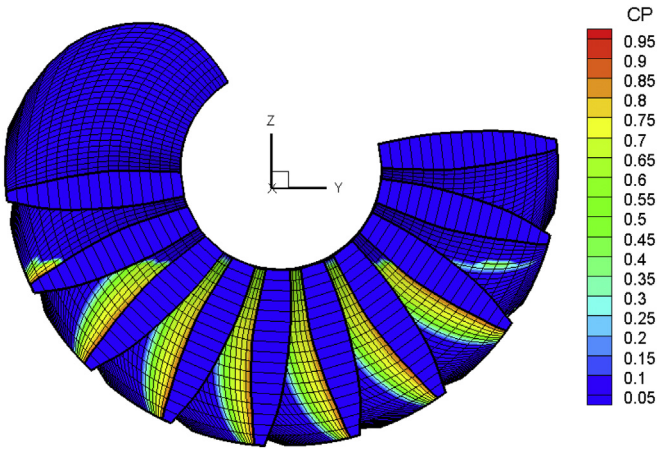

Fig. 8. Contour of pressure coefficients in J = 0.5 and Fn = 2 at angular position of Key blade.

$$Re_j = \frac{\rho \,.(V_I)_j \,.\, C_j}{\mu} \tag{27}$$

Where μ is the dynamic viscosity of fluid.

The non-dimensional hydrodynamic coefficients (thrust coefficient K_T and torque coefficient KQ) of the propeller are expressed as follows:

$$K_T = \frac{T}{\rho\, n^2 D^4}\,, \quad K_Q = \frac{Q}{\rho\, n^2 D^5}\,, \quad J = \frac{V_A}{n\, D} \tag{28}$$

7. Numerical results

7.1. Grid generation description

Due to the behavior of flow on a SPP is always in unsteady condition and then numerical simulation must be solved marching in time, during a full rotation of the propeller.

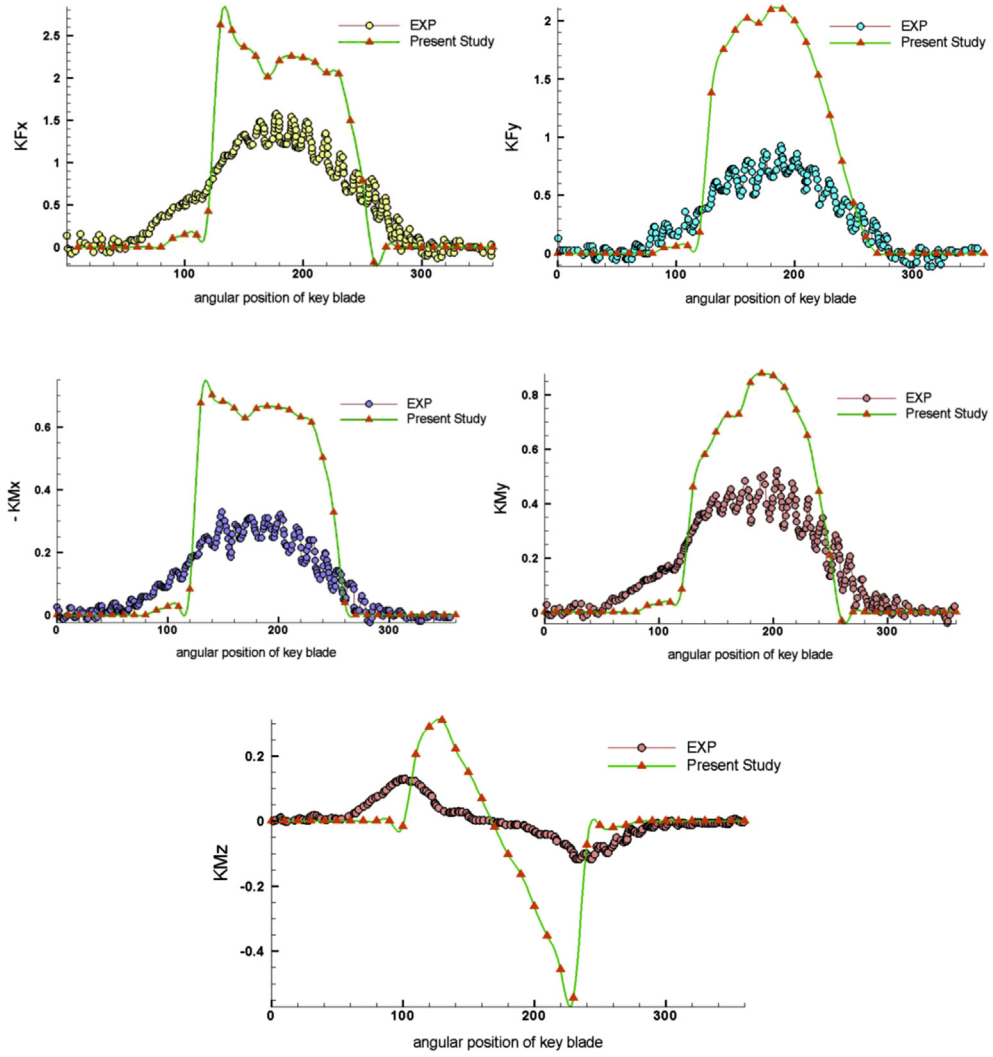

Fig. 9. Comparison between the calculated and measured rotational fluctuation of 5-component force/moment versus angular position of key blade at J = 0.4.

Therefore, grid generation on SPPs is facing with high complexities. There are different methods for grid production on propeller, but the adaptation between grid generation method and solution method in the boundary element method is very important. A conventional grid has been used for propeller blades in this study. Pyo (1995) states that these grids could improve the performance of the BEMs for skewed and highly skewed propellers. Recent studies on the ellipsoid made by Falcão de Campos et al. (2005) reveal that the accuracy of a low-order Morino potential based BEM is higher for conventional grids. Also, based on common practice for propeller design, conventional grids are easier to generate and do not need an extra computational treatment.

In grid generated on SPP as much as possible, the aspect ratio is close to one. After review, assessment and Sensitivity Survey of number of elements in chord and radial directions, adequate number of surface elements on SPPs is produced. Generated geometry of 841-B propeller for analysis using boundary element code is shown in Fig. 5. Since the analysis is in the unsteady condition, so in each time step wake shape is changed. In the following picture at special moment, the wake composed of the key blade is shown. In this work the classic trailing wake geometry is enforced, which requires zero pressure jump across the wake sheet. Cup of blade increases the propeller pitch on PSP and super-cavitating propellers, thus this ability there's that the wake alignment behind the PSP blade in low propeller pitch can be modeled using the classic trailing wake geometry compared with Greeley's model.

7.2. Solution algorithm description

For surface-piercing propellers, second identity Green's equation is solved for the total number of sub-merged panels

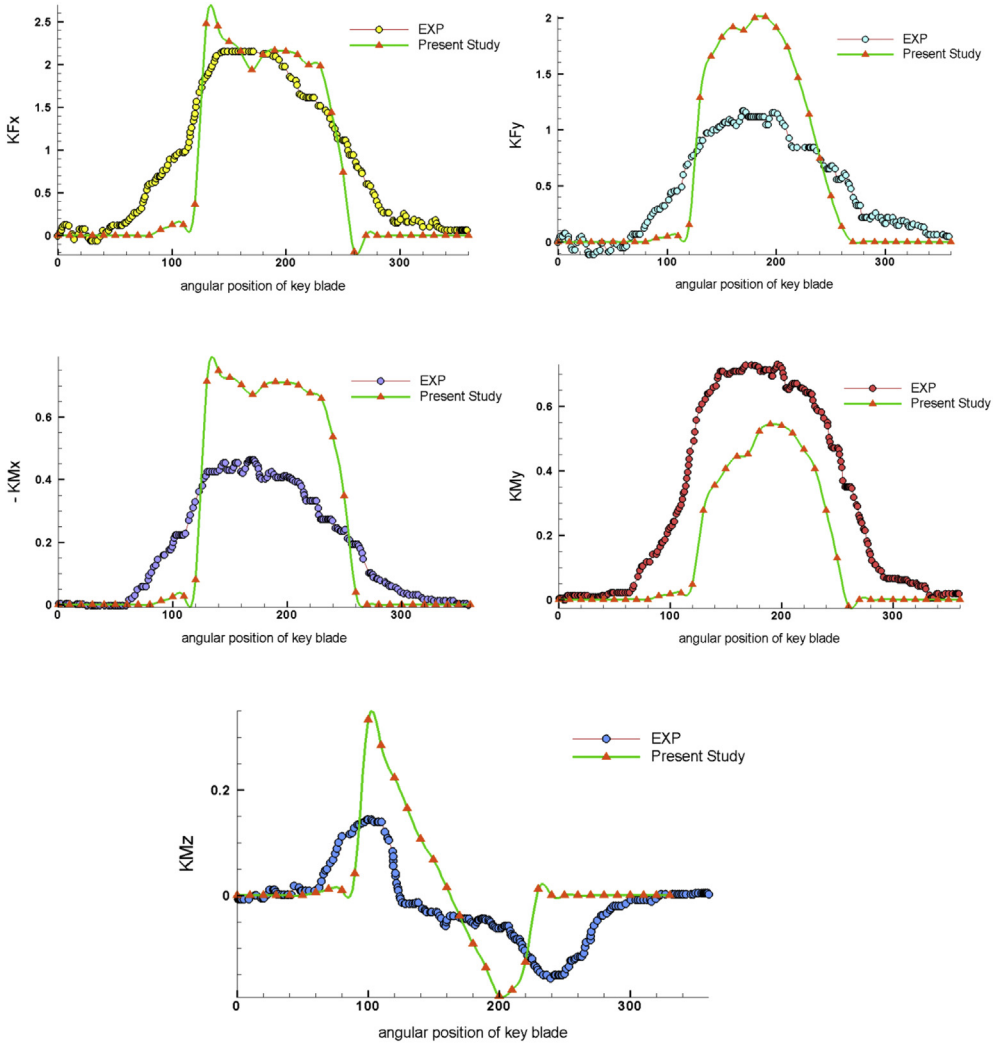

Fig. 10. Comparison between the calculated and measured rotational fluctuation of 5-component force/moment versus angular position of key blade at J = 0.5.

and the ventilating surface of the key blade. The values of all boundary conditions are set equal to zero on the blade and wake panels that are above the free surface. For the unsteady flow model one propeller rotation or cycle is discretized in N_t time steps Δt, or angular steps $\Delta\theta$. The algorithm of the complete iterative process can be divided in three different parts: preparation loop, iterative process and convergence testing. In the preparation loop an initial guess for the loading $\Delta\phi$ is obtained from the simple Morino-Kutta condition, as well as the pressure jump ΔC_p. The reduced system matrices Eq. (23) and Jacobian matrix are calculated. This is done outside the iterative loop. This loop involves the Newton step calculation and finally the pressure jump calculation. Convergence is achieved if $max\left|\Delta C_p\right| < \varepsilon$ being a prescribed tolerance. Also, if $max\left|\Delta C_p^{n+1}\right| < max\left|\Delta C_p^{n}\right|$ it means that the minimization direction is the correct one and therefore we can keep the Jacobian matrix fixed from the previous iteration in order to save CPU time. Otherwise a new Jacobian matrix is recomputed. An additional check is performed in order to add some robustness to the algorithm.

7.3. Validation with experiments

In order to validate the treatment of surface piercing propellers, numerical predictions for SPP-841B propeller model are compared with experimental measurements collected by Olofsson. A photograph of the partially submerged propeller ventilation and the corresponding boundary element method contours are compared. For the comparison numerical results with experimental data by Olofsson, the flow conditions in each advance ratio were set as shown in Table 2. To study the behavior of flow around SPP, numerical analysis is done in the

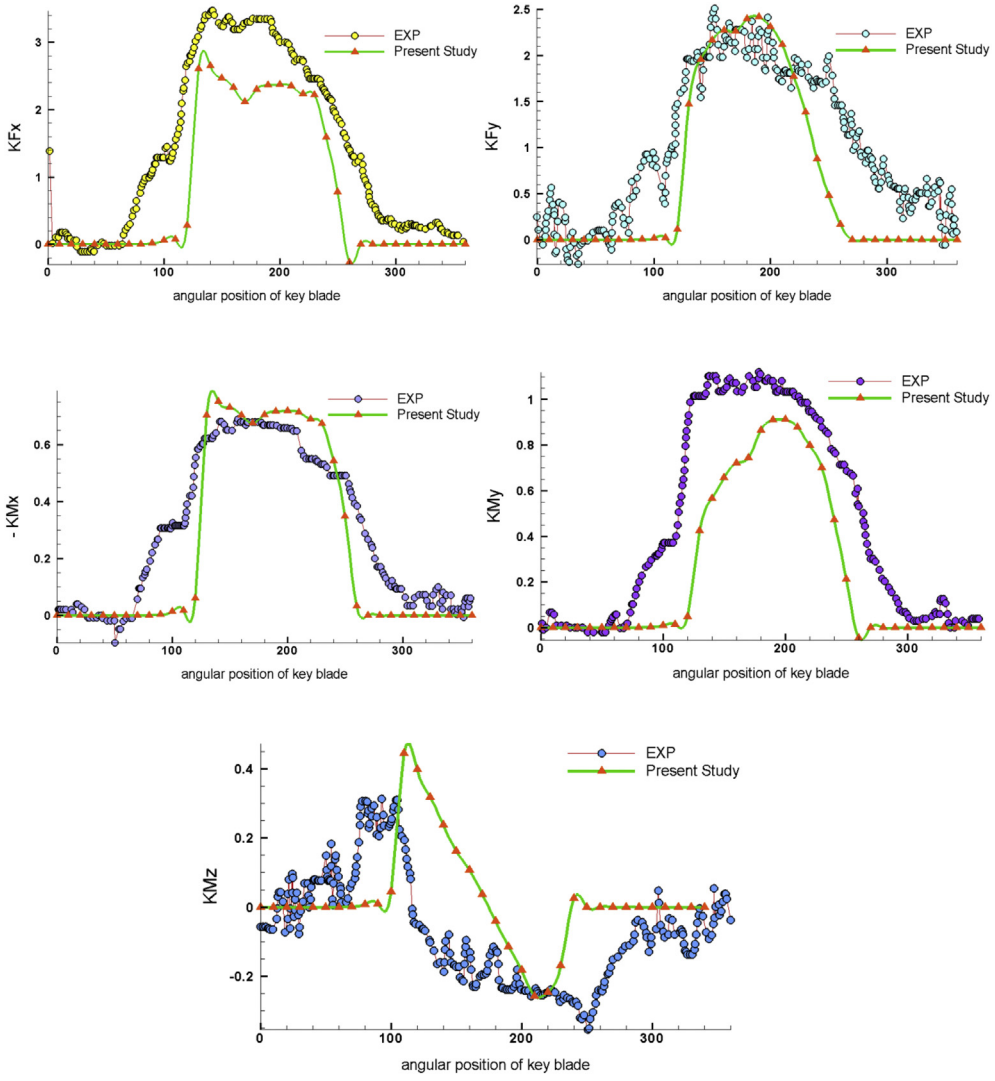

Fig. 11. Comparison between the calculated and measured rotational fluctuation of 5-component force/moment versus angular position of key blade at J = 0.7.

lower and higher advance coefficients than design point of the SPP. For validate the performance prediction of the BEM, convergence studies with varying panel discretization and time step size are presented in this section. All the convergence studies shown in this section are for propeller model 841-B with J = 0.5. Fig. 6 depicts the influence of panel discretization on the individual blade forces, which also converged quickly with number of panels. Because the size of the grid generated on the propeller for analysis using the boundary element method is deeply dependent to the propeller diameter and the aspect ratio of produced elements. Given that in the present study the propeller diameter is small, thus can be seen that with the small number of elements, but with the aspect ratio close to one, the convergence has rapidly occurred. In Fig. 7, the convergence of the individual blade forces at different $\Delta\theta$ are presented. Notice that the result also converged quickly with time step size. In continue, test conditions, and comparisons of predictions with experimental measurements are presented.

In Fig. 8, the contour of the pressure coefficient on the 841-B surface piercing propeller is shown in several different positions during angular rotation of key blade.

Comparison between simulated and measured 841-B propeller open water characteristics is shown in continue. Similarly, comparisons of 5-component force/moment coefficients at low and high advance coefficients are shown in Fig. 9 until Fig. 14. Experimental data correspond to the flow conditions using for BEM simulations shown in Table 2. In this Figures the fluctuations of three components of forces/moments of key blade of the propeller in compare with the experimental results are plotted. As can be seen both numerical and experimental curves have the same procedures. But in some cases, numer-

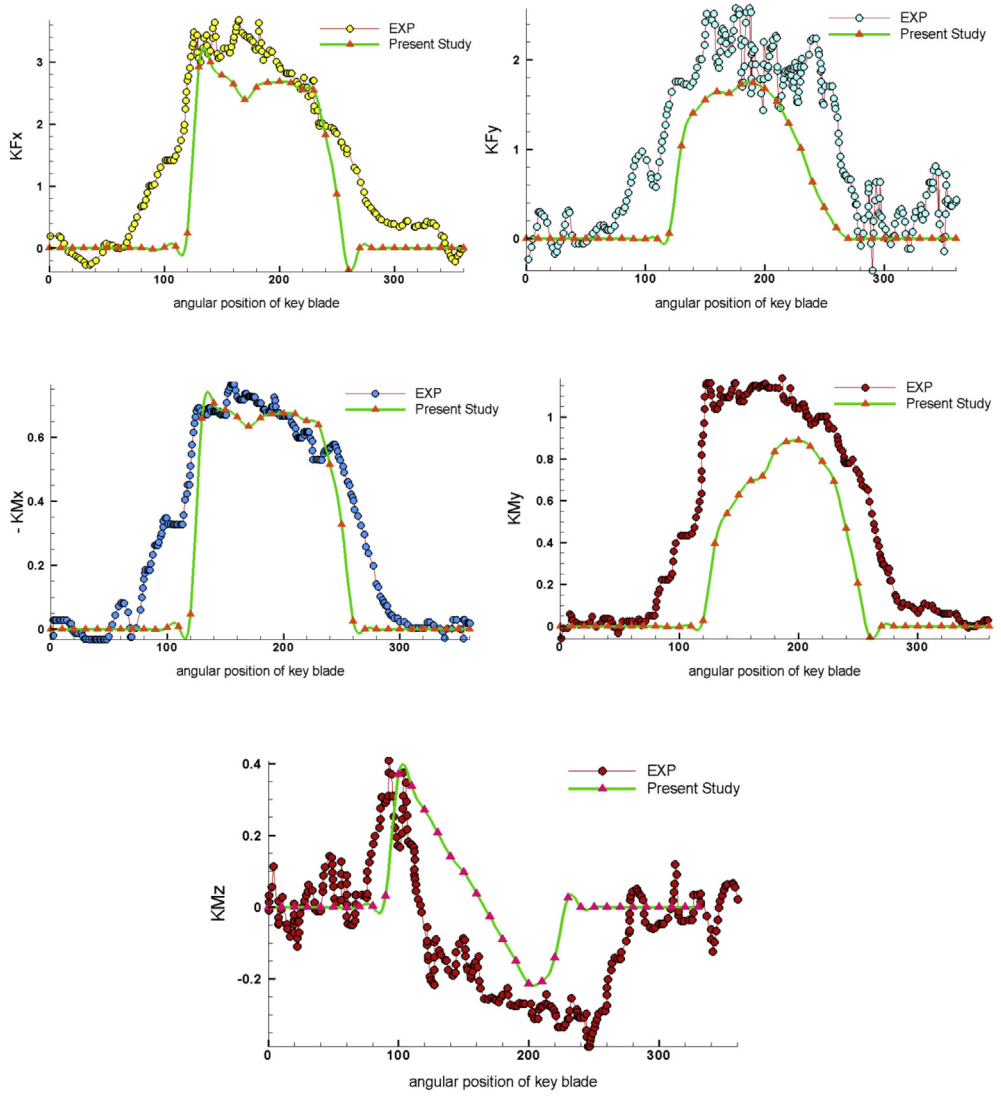

Fig. 12. Comparison between the calculated and measured rotational fluctuation of 5-component force/moment versus angular position of key blade at J = 0.8.

ical results are much larger than experimental data. The error is due to the using of image method and removed the effect of free surface. A nonlinear free surface model should be applied to capture the development of the jet, so that the added hydrodynamic force can be directly evaluated. The overall free surface rises due to the ventilation displacement effect Olofsson (1996). As a result, the actual immersion of the propeller increases, which in turn adds to the hydrodynamic blade load. In the other words, due to the instability in the transition region, in particular in the low advance coefficients, the numerical modeling of flow well not have the ability to show fluctuations (see Fig. 10–13).

By averaging the fluctuations of force and moment about the x-axes after some rotations, KT and KQ were calculated. According Figs. 15 and 16 simulation results had very good agreements with experimental measurements in high advance coefficients. Because usually the maximum efficiency is related to the design point of propeller, therefore, at this point the maximum coincidence can be seen between the numerical and experimental results. In low advance ratios, less than number one, greater difference can be seen that related to operation of SPP in heavy condition.

Fig. 17 shows the percentage error of numerical obtained results compare with experimental data. According to the figure, the results of numerical simulations agreed with the experimental measurements well in high advance coefficients and the maximum error are less than 2%. Increase the error rate in advance coefficients down because of working of propeller in heavy condition.

In Figs. 18 and 19 ventilation pattern on the back side of key blade of the SPP during rotation is shown in three different positions. This results are for the J = 1.2 and J = 0.8 and as can be seen, there are fairly good conformity between experimental observation and numerical contours.

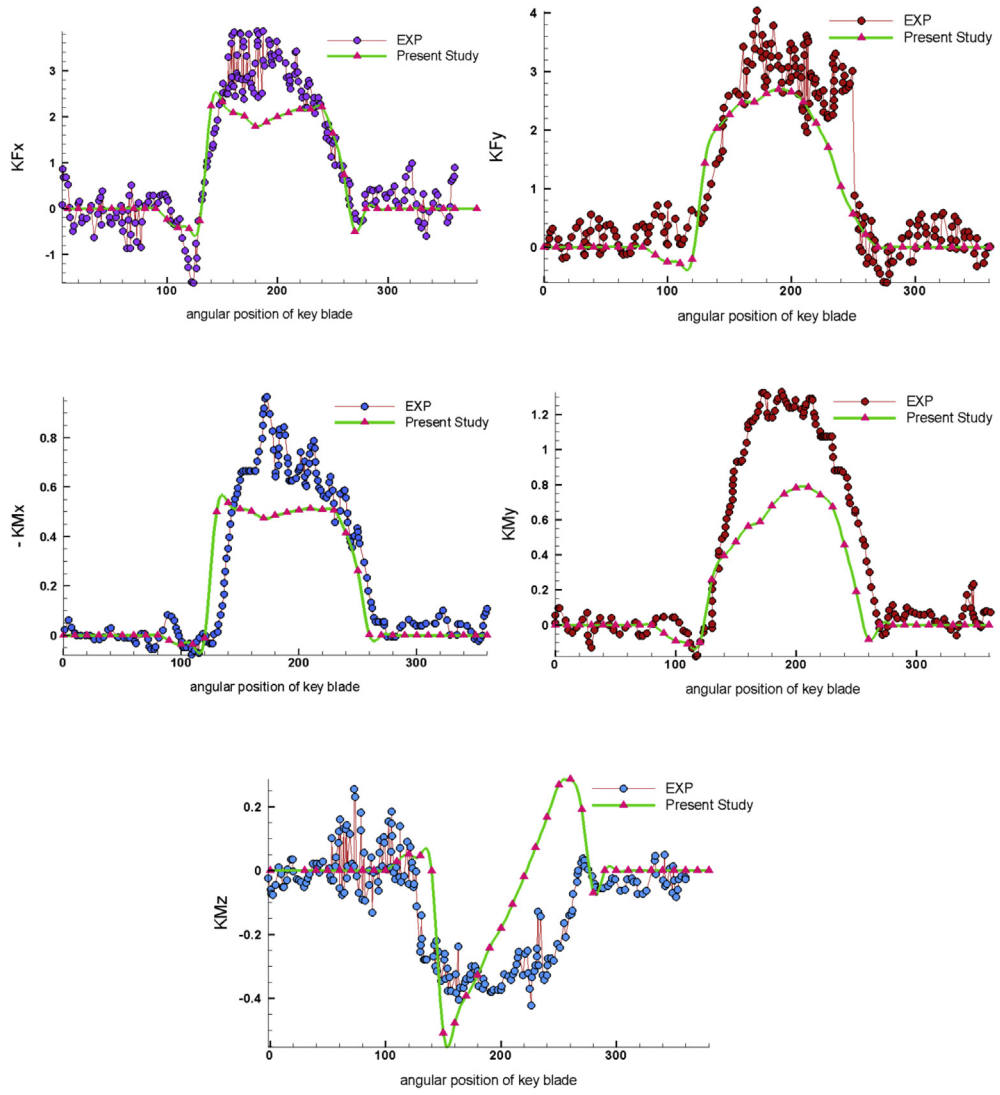

Fig. 13. Comparison between the calculated and measured rotational fluctuation of 5-component force/moment versus angular position of key blade at J = 1.1.

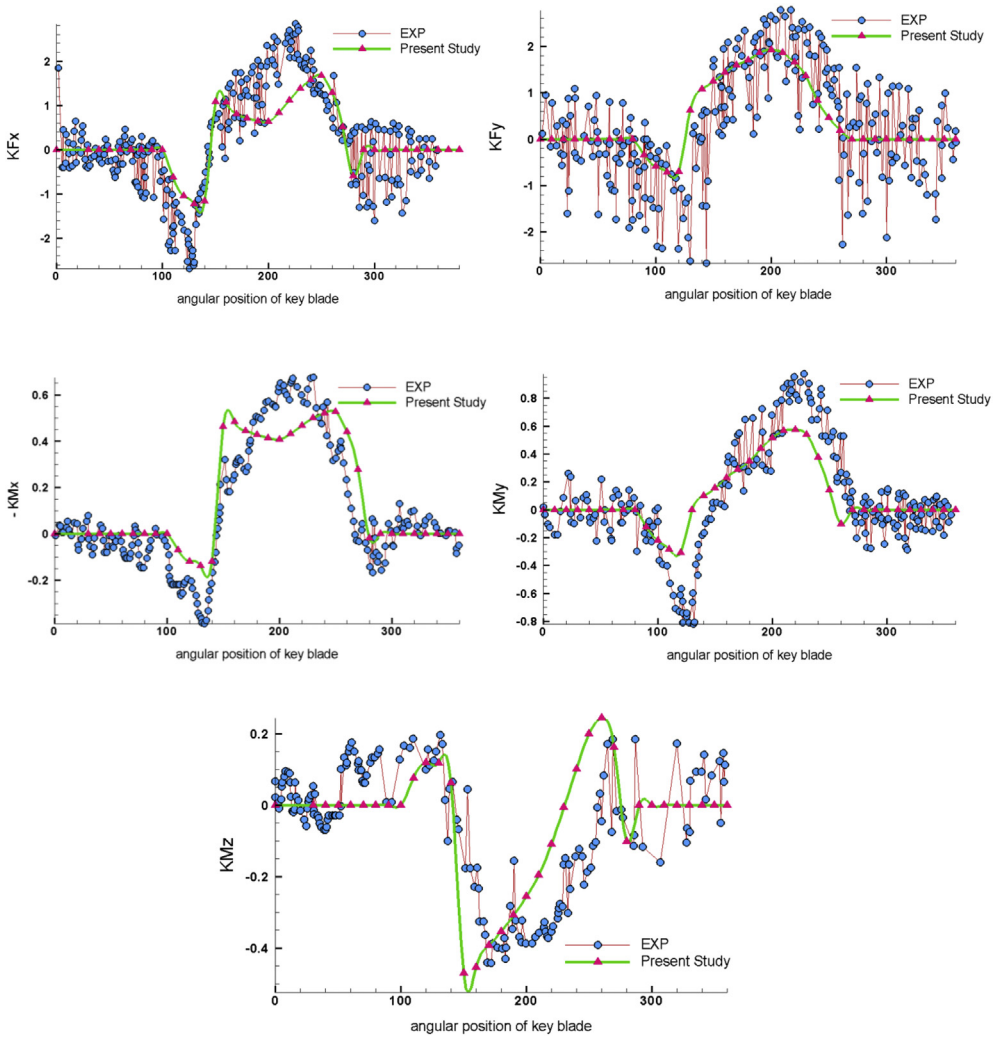

Fig. 14. Comparison between the calculated and measured rotational fluctuation of 5-component force/moment versus angular position of key blade at J = 1.3.

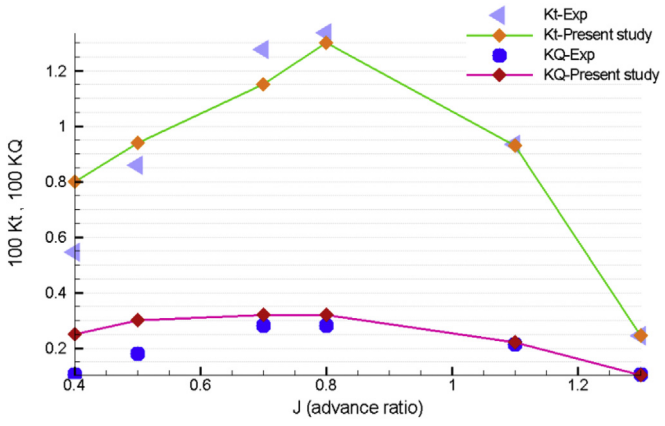

Fig. 15. Comparison between the calculated and measured K_T, KQ.

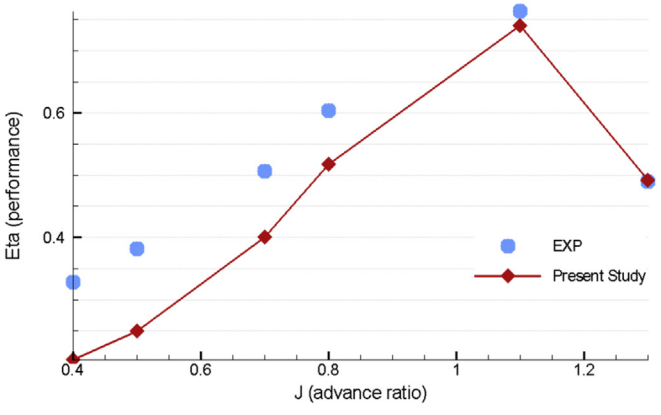

Fig. 16. Comparison between the calculated and measured η_O.

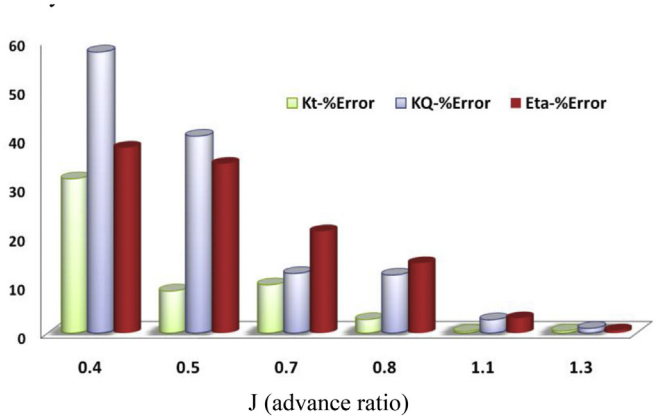

Fig. 17. Relative percentage error versus advance coefficients.

8. Conclusions

The objective of this study was to use the boundary element method simulation for analysis of the SPP so as to be able to study physical phenomena relevant to SPP and its design for a given operating condition. According to the obtained results, numerical calculation both in terms of forces/moments and the predicted ventilation patterns agree well with experiments measurements. The trailing edge and cup of blade have a significant impact in increasing of static pressure of face side. Also cup of blade prevent from spraying water into the air that don't investigated in this study. However, there are some discrepancies between the predicted and measured individual blade forces, particularly at low advance coefficients. Among the difference factors is that a linear free surface model has

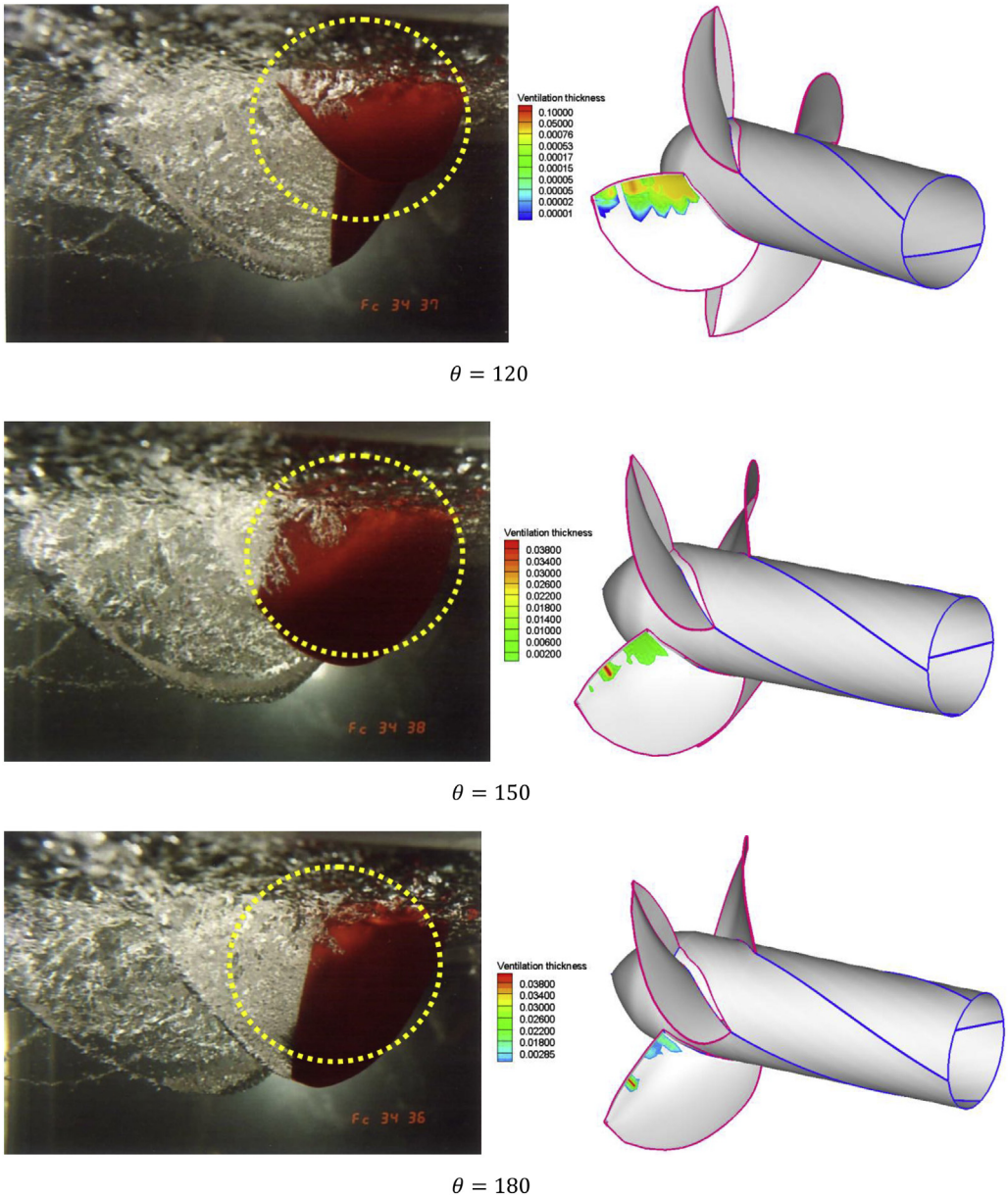

Fig. 18. Comparison of the observed and simulated ventilation patterns at J = 1.2, Fn = 2.

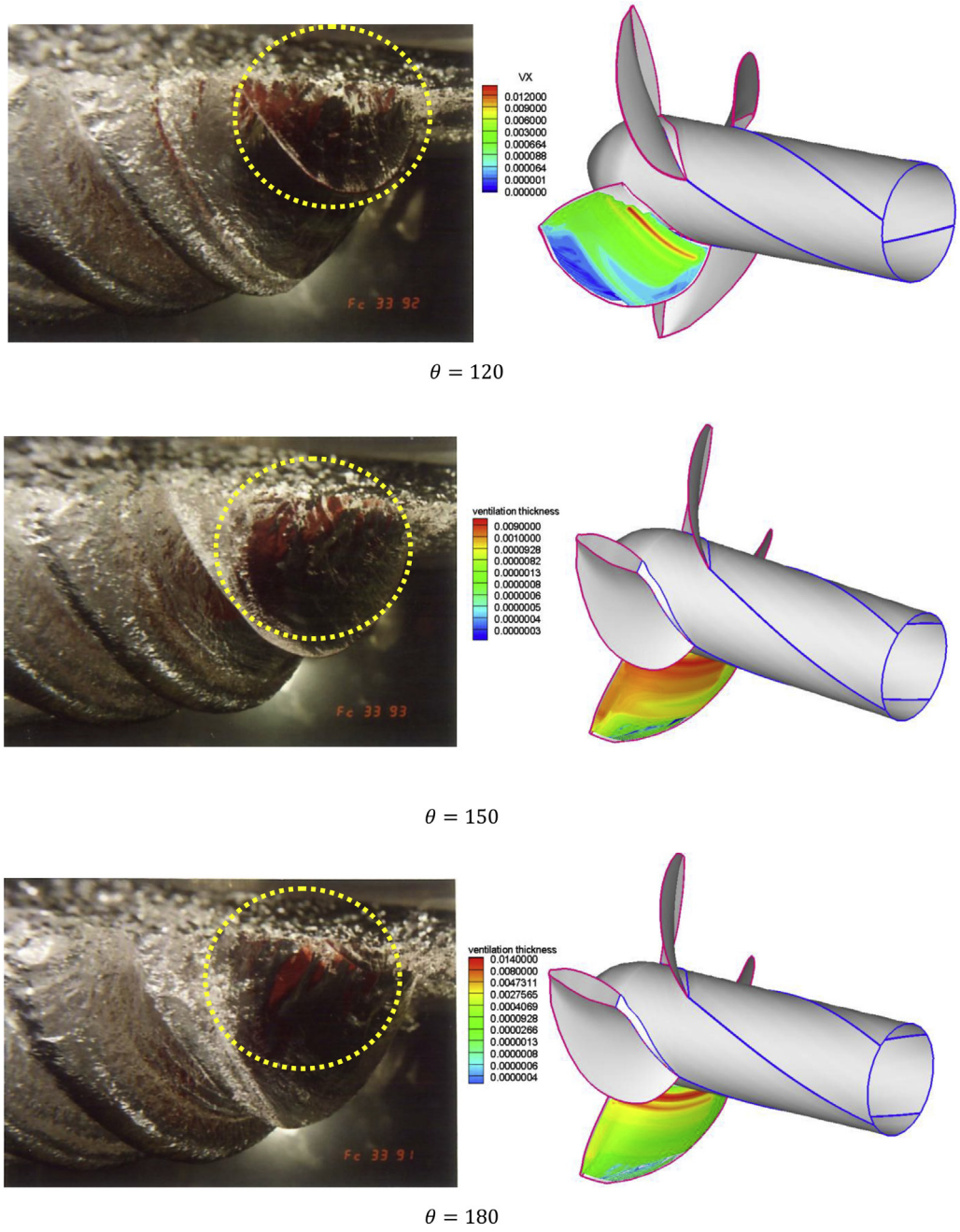

Fig. 19. Comparison of the observed and simulated ventilation patterns at J = 0.8, Fn = 2.

been applied in this study, so that the added hydrodynamic force cannot be evaluated. The overall free surface rises due to the ventilation displacement effect, but in the present study due to the using of image method the effect of free surface has been removed.

References

Califano, A., Steen, S., 2009. Analysis of different propeller ventilation mechanisms by means of RANS simulations. In: First International Symposium on Marine Propulsors, SMP'09, Rondheim, Norway, June.

Falcão de Campos, J.A.C., Sousa, P., Bosschers, J.A., 2005. Verification study on low-order three-dimensional potential based panel codes. Comput. Fluids 35, 61–73.

Fine, N., 1992. Non-linear Analysis of Cavitating Propellers in Non-uniform Flow (PhD thesis). Massachusetts Institute of Technology.

Furuya, O., 1985. A performance prediction theory for partially submerged ventilated propellers. J. Fluid Mech. 151, 311–335.

Ghassemi, H., December 2009. Hydrodynamic characteristics of the surface-piercing propellers for the planing craft. J. Mar. Sci. Appl. 8 (4), 267–274.

Hadler, J., Hecker, R., 1968. Performance of partially submerged propellers. In The 7th ONR Symposium on Naval Hydrodynamics. Rome, Italy.

Hess, J.L., Valarezo, W.O., 1985. Calculation of steady flow about propellers using a surface panel method. J. Propuls. Power 1 (6), 470–476. http://dx.doi.org/10.2514/3.22830.

Himei, Kohei, 2013. Numerical analysis of unsteady open water characteristics of surface piercing propeller. In: 3rd International Symposium on Marine Propulsors SMP'13, Launceston, Tasmania, Australia, pp. 292–297.

Hsin, C., 1990. Development and Analysis of Panel Methods for Propellers in Unsteady Flow (PhD thesis). Massachusetts Institute of Technology.

Huang, S., Wang, P.S., Hu, J., 2007. A method for numerical calculation of propeller hydrodynamics in unsteady inflow. J. Mar. Sci. Appl. 6 (2), 6−11.

Kim, Y.G., Lee, C.S., 1996. Prediction of unsteady performance on marine propellers with cavitation using a surface panel method. In: Proceedings of the 21st Symposium on Naval Hydrodynamics.

Kim, Y.G., Lee, C.S., Suh, J.C., 1994. Surface panel method for prediction of flow around 3D steady or unsteady cavitating hydrofoil. In: Proceedings of the 2nd International Symposium on Cavitation.

Kinnas, S.A., Fine, N.E., 1990. Non-linear analysis of the flow around partially or super-cavitating hydrofoils by a potential based panel method. In: IABEM90 Proceedings, Rome, Italy.

Kinnas, S.A., Fine, N.E., 1992. A nonlinear boundary element method for the analysis of unsteady propeller sheet cavitation. In: Proceedings of the 19th Symposium on Naval Hydrodynamics, Seoul, Korea, pp. 717−737.

Kinnas, S., Young, Y.L., Lee, H., Gu, H., Natarajan, S., 2003. Prediction of cavitating flow around a single or two-component propulsors, ducted propellers and rudders. In: CFD2003 Proceedings, London, UK.

Koushan, K., 2004. Environmental and interaction effects on propulsion systems used in dynamic positioning, an overview. In: Proceedings of 9th International Symposium on Practical Design of Ships and Other Floating Structures PRADS 2004, Lübeck-Travemünde, Germany.

Kozlowska, A.M., Wöckner, K., Steen, S., Rung, T., Koushan, K., Spence, S., 2009. Numerical and experimental study of propeller ventilation. In: First International Symposium on Marine Propulsors, SMP'09, Trondheim, Norway.

Kruppa, C.F.L., 1992. Testing surface piercing propellers. Hydrodyn. Comput. Model Tests Real. 107−113.

Lee, C.S., Kim, Y.G., Lee, J.T., 1992. A potential based panel method for the analysis of two-dimensional super or partially cavitating hydrofoil. J. Ship Res. 2 (36).

Lee, H., Kinnas, S., Gu, H., Natarajan, S., 2003. Numerical modeling of rudder sheet cavitation including propeller/rudder interaction and the effects of a tunnel. In: Cav2003 Proceedings, Osaka, Japan.

Lee, H.S., Kinnas, S.A., 2002. Application of BEM in unsteady blade sheet and developed tip vortex cavitation prediction on marine propellers. In: IABEM 2002 Proceedings, Austin Texas, USA.

Lee, J., 1987. A Potential Based Panel Method for the Analysis of Marine Propellers in Steady Flow (PhD thesis). Massachusetts Institute of Technology.

Misra, S.C., Gokarn, R.P., Sha, O.P., Suryanarayana, C., Suresh, R.V., 2012. Development of a four-bladed surface piercing propeller series. Nav. Eng. J. 124-4, 105−138.

Mueller, A.C., 1998. Development of Face and Mid-Chord Cavitation Models for the Prediction of Unsteady Cavitation on a Propeller (Master's thesis). The University of Texas at Austin.

Oberembt, H., 1968. Zur bestimmung der instationären flügelkräfte bei einem propeller mit aus dem wasser herausschlagenden flügeln. Technical report. Inst.fur Schiffau der Universitat Hamburg. Bericht Nr. 247.

Olofsson, N., 1996. Force and Flow Characteristics of a Partially Submerged Propeller (PhD thesis). Department of Naval Architecture and Ocean Engineering, Chalmers University of Technology, Goteborg, Sweden.

Pellone, C., Pellat, J., 1995. Nonlinear analysis of three-dimensional partially cavitating hydrofoils. In: Proceedings of the Cav95 International Symposium on Cavitation.

Pellone, C., Rowe, A., 1981. Supercavitating hydrofoils in nonlinear theory. In: Proceedings of the 3rd International Conference on Numerical Ship Hydrodynamics. Paris, France.

Pyo, S., 1995. Numerical Modeling of Propeller Tip Flows with Wake Sheet Roll-up in Three Dimensions (PhD thesis). Massachusetts Institute of Technology.

Rose, J.C., Kruppa, C.F.L., 1991. Surface piercing propellers − methodical series model test results. In: FAST'91, Norway.

Rose, J.C., Kruppa, C.F.L., Koushan, K., 1993. Surface piercing propellers − propeller/hull interaction. In: FAST'93, pp. 867−881. Japan.

Savineau, C.M., 1996. A Time Marching Boundary Element Method for the Prediction of the Flow Around Surface Piercing Hydrofoils (Master's thesis). Department of Ocean Engineering, Massachusetts Institute of Technology. February.

Savineau, C., Kinnas, S.A., 1995. A numerical formulation applicable to surface piercing hydrofoils and propellers. In: 24th American Towing Tank Conference. Texas A&M University, College Station, TX.

Shiba, H., 1953. Air-Drawing of Marine Propellers. Technical Report 9. Transportation Technical Research Institute.

Uhlman, J.S., 1987. The surface singularity method applied to partially cavitating hydrofoils. J. Ship Res. 2 (31), 107−124.

Vinayan, V., Kinnas, S.A., 2008. Numerical modeling of surface piercing hydrofoils and propellers. In: Proceedings of the 27th Symposium on Naval Hydrodynamics.

Vinayan, V., Kinnas, S.A., 2009. A boundary element method for the strongly nonlinear analysis of surface-piercing hydrofoils. In: Proceedings of the 7th International Symposium on Cavitation. CAV2009-Paper No. 97. August 17−22, Ann Arbor, Michigan, USA.

Wang, D., 1977. Water entry and exit of a fully ventilated foil. J. Ship Res. 21, 44−68.

Wang, D., 1979. Oblique water entry and exit of a fully ventilated foil. J. Ship Res. 23, 43−54.

Wang, G., Jia, D., Sheng, Z., 1990. Hydrodynamic performance of partially submerged ventilated propeller. Shipbuild. China 2.

Wang, G., Jia, D., Sheng, Z., 1992. Study on propeller characteristics near water surface. In: The 2nd Symposium on Propeller and Cavitation, pp. 161−168. Hangzhon, China.

Young, Y.L., Kinnas, S.A., 2002. A BEM technique for the modeling of supercavitating and surface-piercing propeller flows. In: 24th Symposium on Naval Hydrodynamics, Fukuoka, Japan.

Young, Y.L., Kinnas, S.A., 2003. Analysis of supercavitating and surface-piercing propeller flows via BEM. Comput. Mech. 32, 269−280. Springer-Verlag.

Young, Y. Lu, 2003. Fluid and structural modeling of cavitating propeller flows. In: Cav2003 Proceedings, Osaka, Japan.